Periodic array of misfit dislocations at the MnAs/GaAs interface studied by synchrotron x-ray diffraction

D. K. Satapathy,* V. M. Kaganer, B. Jenichen, W. Braun, L. Däweritz, and K. H. Ploog
Paul-Drude-Institut für Festkörperelektronik, Hausvogteiplatz 5-7, D-10117 Berlin, Germany
(Received 4 May 2005; published 4 October 2005)

We study the evolution of strain, morphology and interfacial structure during the growth at 250 °C and subsequent annealing of MnAs films on GaAs *in situ* using grazing incidence x-ray diffraction. The MnAs film grows via the formation of relaxed islands which increase in size and finally coalesce to form a continuous film. Early on, an ordered array of misfit dislocations forms at the interface with a spacing of 4.95 ± 0.05 nm, releasing the misfit strain. The Burgers vector of the dislocations lies in the interface plane, and the inhomogeneous strain due to the dislocations is confined to a 1.6 nm thick region near the interface. Annealing enhances the order of the dislocation array and reduces the mosaicity of the MnAs layer. On MnAs/GaAs(113)A, the same mismatch is released by the dislocations with the two times smaller Burgers vectors and the two times smaller spacing, as compared with the MnAs/GaAs(001).

DOI: 10.1103/PhysRevB.72.155303 PACS number(s): 81.15.Hi, 61.10.−i, 68.35.−p

I. INTRODUCTION

The epitaxy of dissimilar materials (extreme heteroepitaxy) is not only interesting for technological applications, but also for basic research. In the design of such heterostructures, the strain and its relaxation at the interface during heteroepitaxy is crucial, since it affects the structural and electronic properties of the overlayer. A strain amounting to several percent, which is commonly found in heterostructures of dissimilar materials, can endanger the structural stability of the layer and hence the desired performance of the device based on this heterostructure. In particular, the fabrication of spintronics devices[1,2] require the integration of a ferromagnetic metal and a semiconductor with an atomically abrupt interface, since the strain field at the interface may scatter and relax the spin of the electron.[3] We therefore need to understand the atomistic processes responsible for the generation of defects during the initial stages of growth as well as the strain relaxation and its distribution, both in the interface plane and normal to it at the interface to optimize the spin injection efficiency at such interfaces.

In the present paper we study, by means of *in situ* grazing incidence x-ray diffraction (GID), the process of formation, the structure of the interface, the effect of annealing on the heterointerface and the crystal quality of MnAs epitaxial films on GaAs(001) and GaAs(113)A substrates. In the case of MnAs film growth on GaAs, we observe the formation of relaxed three-dimensional (3D) islands at a nominal thickness of 4.2 ML (1 ML corresponds to 3.2 Å). Generally, the islands may form on the wetting layer in the Stranski-Krastanow growth mode to release the strain or in the Volmer-Weber growth mode, the nonwetting case.[4,5] We cannot make any conclusion about the formation of the wetting layer. However, it is worth to point out that the strain in large Volmer-Weber or Stranski-Krastanow islands is ultimately released by misfit dislocations.

Misfit dislocations in most semiconductor heterostructures are irregularly distributed at the heterointerface, because the dislocation glide planes are usually inclined to the heterointerface and dislocations are generated by extrinsic nucleation.[6] The dislocations are rather immobile in the interface plane and their lateral distribution is mostly determined by the random distribution of the nucleation sources. In contrast to this usually observed behavior, ordered array of misfit dislocations has been found by transmission electron microscopy (TEM)[7] and by GID at the MnAs/GaAs(001) interface.[8] Periodic dislocation arrays can be formed if the dislocation glide plane is parallel to the interface, resulting in a high dislocation mobility along the interface, and assuming a homogeneous nucleation mechanism.[9] Repulsive dislocation interaction gives rise to equal spacings between the dislocations. Periodic arrangements of misfit dislocations are found in several other systems [Ag/MgO (Ref. 10), Fe/W (Ref. 11), PbTe/PbSe (Ref. 9), GaSb/GaAs (Refs. 12 and 13), AlN/Si(111) (Ref. 14)] with high lattice mismatch. As discussed below, these conditions are met for the MnAs/GaAs heterostructures and a highly periodic array of misfit dislocations is formed at the interface. We also observe the periodic dislocations at the MnAs/GaAs(113)A interface with different periodicity.

Molecular beam epitaxy (MBE) growth of high-quality MnAs layers has been reported on different orientations of GaAs [(001), (111), (113)] (Refs. 15–20) and on Si(001).[21] Bulk MnAs crystallizes in the hexagonal NiAs-type structure with the lattice parameters[22] $a=3.72$ Å and $c=5.71$ Å at room temperature. The lattice parameter misfit, f, between MnAs and GaAs along the MnAs$[11\bar{2}0]$ direction (a axis) is $f=(a_f-a_s)/a_f=[d_{\mathrm{MnAs}(11\bar{2}0)}-d_{\mathrm{GaAs}(220)}]/d_{\mathrm{MnAs}(11\bar{2}0)} \simeq -7.5\%$, where a_f and a_s are the epilayer and substrate lattice parameters, respectively. Along the [0001] (c axis) direction, the mismatch is very large $\sim 29\%$. This large mismatch is accommodated by the formation of a coincidence site lattice.[7]

MnAs assumes the NiAs-type γ-MnAs structure above 125 °C, the orthorhombic MnP-type β-MnAs structure between 125 °C and 45 °C, and the ferromagnetic NiAs-type α-MnAs structure below 45 °C.[23] It is therefore difficult to deduce the strain state of the film during epitaxy by *ex situ* measurements at room temperature. Only *in situ* experiments

can provide access to the strain state of the system at the growth temperature during deposition. Grazing incidence x-ray diffraction[24] is well suited for this purpose, since it can be used *in situ* in ultrahigh vacuum, without perturbing the MBE growth. GID also allows the characterization of a dislocation network unambiguously.

In this paper, we first describe the experiment, followed by the results from *in situ* growth of MnAs on GaAs(001). The misfit accommodation at the interface is then discussed for both MnAs/GaAs(001) and MnAs/GaAs(113)A heterostructures. We determine the Burgers vector from the number of satellite peaks present between the layer and substrate reflections. The intensity distributions along the crystal truncation rods (CTRs) of the satellites originating from dislocations are determined. From the intensity decay, we obtain the thickness of the layer having an inhomogeneous strain distribution due to the presence of dislocations at the interface. Finally, we investigate the effect of post-growth annealing on the quality of the crystalline film and the interface between MnAs and GaAs(113)A.

II. EXPERIMENT

The x-ray scattering experiments were performed *in situ*, during and after growth at the PHARAO beamline (U125/2-KMC) at the synchrotron BESSY in Berlin, Germany, using a six-circle diffractometer operating in the *z*-axis mode. At this beamline, a multi-solid-source MBE chamber is permanently installed within the diffractometer.[25] In the exit beam path, the MnAs growth chamber has a $100°$(azimuthal) $\times 45°$(polar) beryllium window, allowing access to a significant fraction of reciprocal space. The angular resolution of the detector is defined by two sets of 2×2 mm^2 slits at distances of 200 mm and 1100 mm from the sample. A monochromatic x-ray beam of either 12 or 10 keV energy is used. The grazing incidence angle α_i is kept close to the angle of total external reflection to suppress thermal diffuse scattering from the substrate.

In-plane scans were performed in a grazing incidence—grazing exit geometry. The scan geometry along the MnAs$[11\bar{2}0]$ direction is shown schematically in Fig. 1. The reference frame is chosen such that the in-plane h and k axes are along GaAs[100] and GaAs[010], respectively. In this sketch, the arrow indicates the scan direction. The large circles represent the integer-order GaAs reflections. The squares represent the reflections of the relaxed MnAs film. The solid circles correspond to the satellite reflections due to the dislocation array observed in the measurements and discussed below in detail. All reflections are extended in the surface normal direction due to the finite film thickness.[26]

For this study we have grown MnAs films on the GaAs(001) and (113)A surfaces by solid source MBE chamber described above. Prior to the deposition of MnAs on GaAs(001), a thick buffer layer was grown which showed a clear GaAs $\beta(2\times 4)$ reconstruction at the growth temperature of 550 °C. Then, the substrate was cooled to 250 °C, resulting in a GaAs $c(4\times 4)$-reconstructed surface[27] that was used as the growth template for MnAs.[17] The MnAs layer

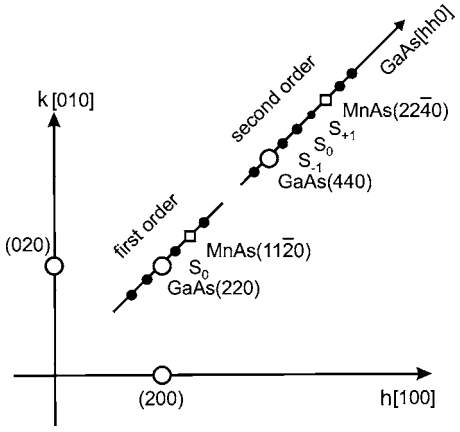

FIG. 1. Schematic representation of the (hk0) reciprocal space plane of MnAs/GaAs(001) with an array of misfit dislocations at the interface. The large open circles and the squares correspond to the GaAs and MnAs Bragg peaks, respectively. The filled circles represent the position of observed satellite reflections from the dislocation array along GaAs[110]. Two orders of scans with all observed reflections are included.

was grown in an As-rich environment at a substrate temperature of 250 °C with a growth rate of 6 nm/h. The time required for one in-plane scan with good signal to noise ratio is about 6 to 7 minutes. Therefore, between two consecutive scans the increase in thickness is about 6–7 Å(2 ML). The sample was annealed at 400 °C after growth in order to improve the structural quality. The thickness of the MnAs film was about 51 nm obtained from *ex situ* x-ray reflectivity measurement. We estimate a 4% error in thickness measurement.

On GaAs(113)A, the growth of MnAs was started on the (8×1)-reconstructed[28] surface at 240 °C. The sample was annealed after deposition in order to optimize the structural quality of the film. The final thickness of the film was about 75 nm obtained from *ex situ* x-ray reflectivity measurements.

III. RESULTS AND DISCUSSION

A. *In situ* measurements during growth: Structure and morphology

GID measurements and reflection high-energy electron diffraction (RHEED) indicate that MnAs grows in a hexagon-on-cube orientation with the epitaxial relationship MnAs$[11\bar{2}0]\|$GaAs[110] and MnAs$[1\bar{1}00]\|$GaAs[001]. The evolution of strain, island size and microstructure during growth was analyzed in our previous publications.[8,29] We briefly summarize the important findings that are relevant for the results shown here and present the evolution of in-plane mosaicity of the film. The growth of MnAs on GaAs(001) is monitored *in situ*, starting from 1.8 ML up to a thickness of 159 ML by recording radial ($\omega-2\theta$) profiles during growth at various film thicknesses (Fig. 2).

The MnAs$(11\bar{2}0)$ peak is first detected at a nominal layer thickness of 4.2 ML. The peak appears very close to the bulk MnAs position, indicating that MnAs is almost relaxed as

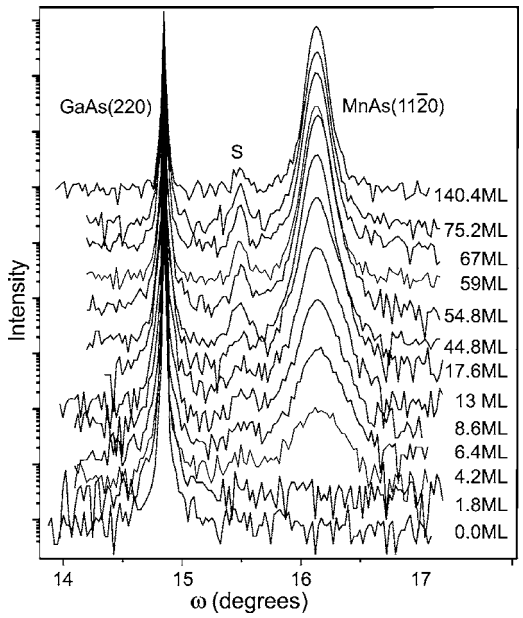

FIG. 2. X-ray diffraction curves ($\omega/2\Theta$ scans) measured *in situ* during growth at 250 °C along the GaAs[110] direction. The scan includes the GaAs(220) substrate and the MnAs(11$\bar{2}$0) layer reflections. The scans are recorded at a grazing incidence angle of 0.2°. The deposited number of monolayers is indicated to the right of each scan. The curves are shifted vertically for clarity. X-ray energy, 12 keV.

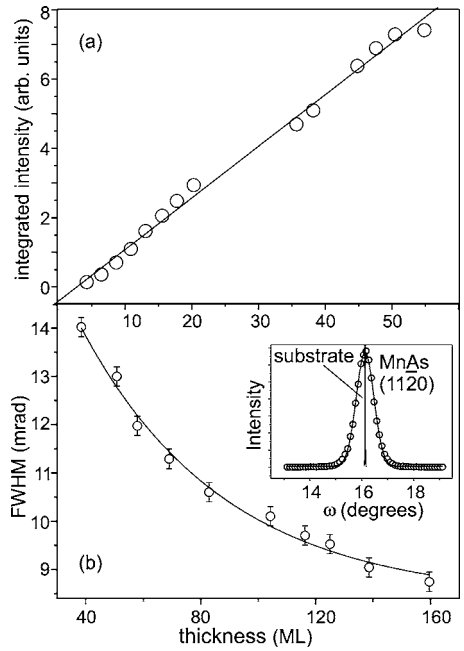

FIG. 3. (a) Evolution of the integrated intensity of the MnAs(11$\bar{2}$0) peak as a function of layer thickness. The solid line is a linear fit to the measured data. (b) The ω-scan width of MnAs(11$\bar{2}$0) as a function of layer thickness. The error bars indicate the accuracy of each data point. The solid line shows an exponential decay fit to the measured data. The inset shows a single transverse scan with the corresponding Gaussian fit. The resolution-limited substrate GaAs(220) peak is also shown in the inset. For clear comparison of widths the GaAs peak is shifted to the center of the MnAs(11$\bar{2}$0) peak.

soon as the MnAs structure is formed. Only 0.1% relaxation of the in-plane lattice spacing a is observed upon further growth until 159 ML. It reaches the value of 3.695 Å at a thickness of 20 ML, after which it remains constant until the final thickness of 159 ML. The layer is almost completely relaxed at the growth temperature. MnAs grows on GaAs with the formation of relaxed three-dimensional islands that subsequently coalesce. We do not see any broadening of the substrate reflection at the beginning of growth (Fig. 2). The absence of the MnAs(11$\bar{2}$0) peak for films less than 4 ML thickness does not necessarily mean that MnAs is growing pseudomorphically on GaAs. Therefore, it is difficult to make conclusions about the presence or absence of a wetting layer. The final lateral island size is estimated to be 27 nm along the MnAs[11$\bar{2}$0] direction by using Scherrer's formula.[30] The islands grow fast until a nominal thickness of 20 ML and slowly afterwards. We therefore conclude that the film becomes connected and continuous at a thickness of about 20 ML. During the deposition, the integrated intensity of the MnAs(11$\bar{2}$0) peak increases linearly with film thickness as shown in Fig. 3(a). This is consistent with kinematical x-ray theory, in which the scattered intensity is proportional to the number of scatterers. This allows us to establish a linear relationship between growth time and film thickness.

A satellite reflection in between the substrate peak and the layer peak (denoted by "S" in Fig. 2) already appears at a nominal layer thickness of about 6 ML. As discussed in the next section, this peak indicates a regular array of misfit dislocations at the interface. Therefore, we conclude that the misfit dislocations form directly at the interface and rearrange to form the periodic structure during growth of the islands before coalescence. To study the evolution of the in-plane mosaic spread of the film after coalescence as a function of layer thickness, in-plane transverse scans are measured *in situ* during growth. Two crystallographic parameters of the MnAs islands, their range of twist and tilt with respect to the surface normal, are used to describe the mosaicity of the film. While the latter is routinely obtained from the widths of x-ray rocking curves of symmetric Bragg reflections, the former is difficult to measure in a conventional laboratory diffraction geometry. An in-plane transverse scan[44] in grazing incidence geometry directly determines the in-plane mosaic spread of the film. One such transverse scan is shown as an inset in Fig. 3. The resolution-limited substrate peak GaAs(220) is shown for comparison. The substrate peak is almost 65 times narrower than the layer peak, demonstrating the high resolution of our experiment. The total width of the rocking curves is affected by the finite size of crystallites and by the in-plane mosaic spread of the film. To separate the two contributions,[31] we use a Williamson-Hall plot.[32] We measure two successive order (11$\bar{2}$0) and (22$\bar{4}$0) peaks of MnAs film. The measured profiles are well fitted with the Gaussian function. The apparatus function is measured separately and approximated to be a Gaussian function of width 0.05°. It is subtracted from the measured width of the MnAs film peaks. From the Williamson-Hall

plot we find that the size contribution to the width of the peak is negligible. The width of the transverse scans is almost entirely due to in-plane mosaic spread. The in-plane mosaic spread decreases down to 8 mrad with increasing layer thickness and can be fitted well by an exponential decay model.

B. Investigation of the MnAs/GaAs(001) interface

1. Observation of the dislocation array

To study the MnAs/GaAs(001) interface, we vary the penetration depth of the x rays by changing the incidence angle α_i of the primary beam.[33,34] For the 10 keV x rays used, the critical angle for total external reflection α_c of MnAs is 0.27°. We vary the grazing incidence angle through a range from below α_c to about $2.5\alpha_c$. The structural configuration of the interface is probed by measuring in an in-plane geometry with a small perpendicular momentum transfer, $L=0.05$ reciprocal lattice units (r.l.u.). Here, L is the (continuous) Miller index of the Bragg reflection $[hkL]$. These measurements were performed at room temperature, after a high-temperature anneal of the sample at 400 °C. The MnAs film has undergone the structural phase transition at 45 °C while cooling to room temperature with a cooling rate of 2 °C min^{-1}.

The GID profiles measured at the first-order reflection (see schematics in Fig. 1) along the MnAs$[11\bar{2}0]$ direction are shown in Fig. 4(a). The grazing incidence angles are given to the right of each profile. Clearly visible are the GaAs(220) reflection and a split MnAs$(11\bar{2}0)$ peak. The MnAs$(11\bar{2}0)$ peak is split due to the strain-mediated coexistence of the α- and β-MnAs phases at room temperature.[35,36] The satellite reflections, S_i, are first observed at a grazing incidence angle 0.3°, which is larger than α_c. The intensities of the satellite reflections increase with increasing α_i, which implies increasing penetration depth of the x rays. Higher-order satellites (S_{-3}, S_{+4}) are detected at $\alpha_i > 0.4°$. We conclude that they are not originating from the surface or the near-surface region of the film but rather from the buried interface between MnAs and GaAs. The satellite S_0 is located exactly halfway between the substrate and the layer (middle of α- and β-MnAs) reflection. All the observed satellite reflections are equally spaced.

MnAs is thermodynamically stable on GaAs and the possible formation of another layer at the interface with a different lattice constant can be ruled out.[15,37] Therefore, we attribute the equally spaced satellite reflections to the regularly spaced misfit dislocations formed at the interface. These results agree well with TEM studies on the same material system.[7,38] The diffraction measurement averages over a much larger real-space distance than TEM and is representative of large areas of the sample. The appearance of the satellites in the radial scans along MnAs$[11\bar{2}0]$ proves that the misfit dislocations are periodic in that direction. We did not find similar satellite reflections in measurements along the MnAs[0001] direction (not shown here).

The width of the satellite reflection S_0 in the $\omega-2\theta$ scan measured at $\alpha_i=0.65°$ in Fig. 4(a) is almost half the width of either the α-MnAs or the β-MnAs peak. Therefore, the width of the satellite reflections from the dislocation array is not limited by nonuniform strain of the layer, but dominated by the much higher order of the GaAs substrate. The factor of 2 difference in the width of the satellite reflection and the layer reflection is also measured in the transverse scans. This demonstrates that the dislocation array is generally better ordered than the film itself.

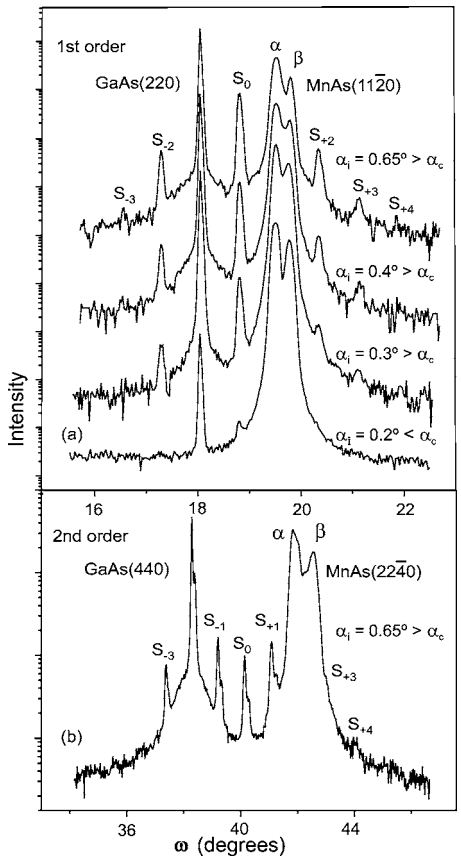

FIG. 4. Radial $(\omega/2\Theta)$ scans recorded along the MnAs$[11\bar{2}0]$ of the MnAs/GaAs(001) heterostructure for different grazing incidence angles α_i. (a) First- and (b) Second-order reflection. The S_i indicate the satellites originating from the periodic array of misfit dislocations. The scans are performed at room temperature. Peaks labelled as α and β refer to the different phases of MnAs. The curves are shifted vertically for clarity. X-ray energy, 10 keV.

2. Period and Burgers vector of the dislocation array

From the period of the satellites in Fig. 4(a), we find the lateral period of the dislocation array, $\Lambda=4.95\pm0.05$ nm, to be comparable to the TEM result, $\Lambda=4.5\pm0.5$ nm.[7] One dislocation every 4.95 nm is sufficient to release the misfit $f=7.5\%$ between the layer and the substrate. The in-plane component of the Burgers vector is $b=\Lambda f=3.71$ Å. It is equal to the a spacing of MnAs, and is given by $\mathbf{b}=\frac{1}{3}[11\bar{2}0]$. This is the shortest possible perfect-dislocation Burgers vector in hexagonal close-packed structures. The line direction of the dislocations is along MnAs[0001], so that the dislocation slip direction is $[11\bar{2}0]$,[39] which means

that it lies in the plane of the interface. In terms of the GaAs lattice, the Burgers vector is equal to GaAs[110].

The number of satellite reflections between the substrate and the layer peaks can be directly related to the Burgers vector. The distance between the substrate and the satellite peaks is $\Delta Q=(2\pi/d)f$, where d is the lattice spacing for the reflection under consideration. The distance between the satellites is $\Delta q=2\pi/\Lambda$. Dividing these quantities and keeping in mind that $\Lambda=b/f$, we obtain

$$\Delta Q/\Delta q = b/d. \quad (1)$$

For the MnAs$[11\bar{2}0]$ reflection, only one satellite S_0 is present halfway between the peaks [see Fig. 4(a)]. Then, $\Delta Q/\Delta q=1/2$ and $b=2d_{(11\bar{2}0)}$. If the Burgers vector would be reduced to half, the satellite spacing would double, and the satellites in the first order reflection would coincide with the main reflections from layer and substrate. The satellite reflections would be observed outside of the main reflections, with the spacing equal to the separation of the main reflections. This situation is realized at the MnAs/GaAs(113)A interface and discussed in Sec. III C. The x-ray diffraction curve along the second-order reflection MnAs$(22\bar{4}0)$ also reveals equally spaced satellite reflections as shown in Fig. 4(b). Now, however, three satellites are present between the main reflections. Equation (1) gives the same Burgers vector $b=4d_{(22\bar{4}0)}=2d_{(11\bar{2}0)}$.

Thus, the MnAs/GaAs(001) interface is appropriate for the formation of a periodic dislocation array. The dislocation density is high due to the large misfit (~7.5% in the a direction of MnAs). The Burgers vector lies in the interface plane, with the slip direction parallel to the interface. This facilitates the glide of the dislocations along the interface. Dislocations nucleate directly at the interface during growth and form a periodic structure even before coalescence (see Fig. 2). At the growth temperature of 250°, the misfit dislocations are mobile and can glide along the interface to form a regular structure to minimize its elastic energy.

The split of the MnAs film peaks due to the strain-mediated coexistence of the α- and β-MnAs phases at room temperature[35,36] is observed in both reflection orders, $(11\bar{2}0)$ and $(22\bar{4}0)$ [see Figs. 4(a) and 4(b)]. In addition to that, the second-order substrate GaAs$(4\bar{4}0)$ peak and the satellite peaks are split. The α-MnAs and β-MnAs domains arrange themselves in a stripe pattern to minimize the elastic energy.[40] The α-MnAs and β-MnAs differ in their in-plane lattice constant by 1.2%. Therefore, the substrate lattice is strained underneath each α and β domain. This modulation leads to two different lattice parameters, which split the GaAs(440) reflection in Fig. 4(b). The splitting is therefore due to the epilayer exerting strain on the substrate. This strain decreases rapidly away from the interface. The penetration of the strain field into the substrate is comparable with the period of the α and β domain stripes, which is about 5 times larger than the film thickness.[36,40] Since the dislocation array is also differently strained by the formation of the domain pattern, the spacing of the dislocations under the α and β domains are slightly different, resulting in a splitting of the satellite reflections. The split of the satellite reflections is comparable to the split of the substrate reflection. Hence, the complete interface structure is modulated by the formation of the α-MnAs and β-MnAs domains.

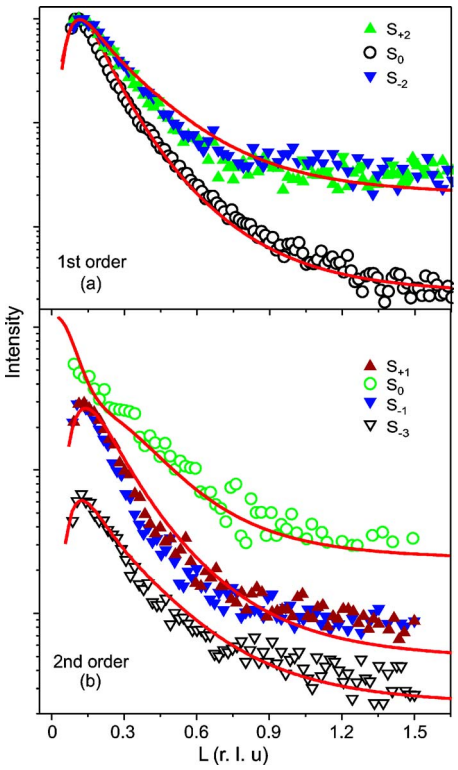

FIG. 5. (Color online) Intensity variation along the crystal truncation rods of different observed satellites originating at the first- and second-order reflection, shown in Figs. 4(a) and 4(b). The continuous (red) lines show the calculated CTRs of the different satellites. No fit parameters are used to match the calculated CTRs with the measured intensity profiles. The profile in (b) is shifted vertically for clarity. X-ray energy, 10 keV.

3. *Truncation rods of the dislocation satellites*

To investigate the variation of strain along the surface normal direction due to the periodic dislocation, we have measured the intensity profiles along the crystal truncation rods (CTRs) of several satellite reflections (hkL) as a function of L. The CTR of a satellite reflection arises from the thin layer at the interface where the strain field due to the dislocations is distributed inhomogeneously. During these measurements, the grazing incidence angle is fixed and the exit angle is varied. The crystal truncation rods of several satellite reflections in the first order [see Fig. 4(a)] are shown in Fig. 5(a). The measured intensity profiles along the CTR of satellites S_{-2} and S_{+2} are very similar. The out-of-plane scattering along each CTR reflects the smoothing of the nonuniform strain when going along the interface normal.

The intensity distribution along a satellite is calculated in the kinematical approximation,

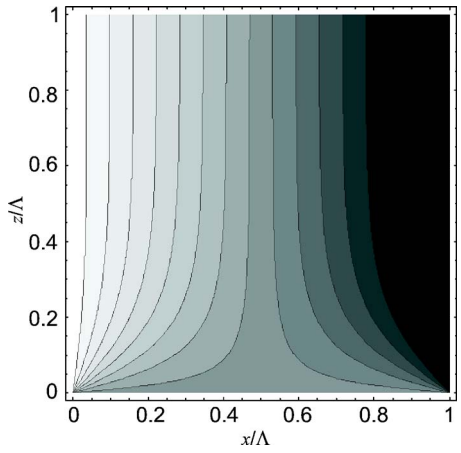

FIG. 6. (Color online) Contour plot of the displacement field due to the periodic dislocations at the interface. Distribution in the plane normal to the surface and normal to the dislocation lines according to Eq. (3). The contour lines are almost parallel to each other for a thickness larger than Λ/π.

$$I_n(q) = \left| \int e^{iQ_n u_x(x,z) + iq_z z} dx dz \right|^2. \quad (2)$$

Here the coordinate x is along the interface in the direction of periodicity and z is the coordinate along the interface normal, $u_x(x,z)$ is the in-plane component of the displacement field of the periodic dislocation array, $q_z = (2\pi/a_s)L$, and $Q_n = (2\pi/\Lambda)n$ (here n is the number of the satellite S_n).

The resulting displacement field due to the periodic array of dislocations is calculated by summing the displacements due to the individual dislocations. The analytical formulas for strain fields of various dislocation arrays can be found in the literature,[39] but the displacement fields are not given. We therefore obtain the displacement field directly by summing the displacement fields of the individual dislocations. The result is

$$u_x(x,z) = \frac{b}{2\pi}\left[\arctan\left(\frac{\tanh(\pi z/\Lambda)}{\tan(\pi x/\Lambda)}\right) + \frac{\pi z/\Lambda}{2(1-\nu)} \frac{\sin(2\pi x/\Lambda)}{\cosh(2\pi z/\Lambda) - \cos(2\pi x/\Lambda)} \right]. \quad (3)$$

In the limit $x, z \ll \Lambda$, this expression reduces to that of individual dislocation. When $z \gg \Lambda/\pi$, Eq. (3) gives rise to a uniform strain $u_{xx} = (b/2\Lambda)\mathrm{sign}(z)$, while the nonuniform strain decays exponentially. Thus, the nonuniform strain is confined to a stripe $|z| < \Lambda/\pi$. The displacement $u_x(x,z)$ calculated by Eq. (3) is shown in Fig. 6. For $|z| > \Lambda/\pi$, the contour lines are almost parallel to each other indicating a constant displacement gradient.

The intensity profiles calculated by Eq. (2) for different satellite reflections are shown as solid lines in Fig. 5(a). Since we are measuring in the regime of small perpendicular momentum transfer (L values below 1.6 r.l.u.), the correction factors to the measured intensity are almost constant in the range considered.[41] We obtain a good agreement between the measured and calculated intensities for different orders of the satellites without introducing any fit parameters (except for scale and background). Figure 5(b) presents the intensity profiles along the CTRs of four satellites ($S_0, S_{\pm 1}, S_{-3}$) of the second-order reflection shown in Fig. 4(b). All the profiles show a similar intensity variation. This demonstrates that they originate from the same thin interfacial layer. The calculated intensity fits well for the different order satellite reflections.

The thickness of the stripe at the interface with inhomogeneous strain ($|z| < \Lambda/\pi$) is directly proportional to the period of the dislocations. For the period of the dislocation array, $\Lambda = 4.95$ nm, we estimate the thickness of the inhomogeneously strained layer of the film to be $\Lambda/\pi = 1.6$ nm. A similar value can be obtained from the full width at half-maximum (FWHM) of the measured intensity of the satellite CTRs.

C. Investigation of the MnAs/GaAs(113)A interface

When growing MnAs on GaAs(113)A, we obtain, from the GID and RHEED measurements, the epitaxial relationships MnAs$[11\bar{2}0] \| $GaAs$(1\bar{1}0)$ and MnAs $\sim(0001) \| $GaAs$(33\bar{2})$. The misfit along the MnAs$[11\bar{2}0]$ direction in the interface between MnAs/GaAs(113)A and MnAs/GaAs(001) is the same -7.5% as on GaAs(001). We therefore expect the same strain relaxation mechanism as for MnAs/GaAs(001), with the formation of a periodic array of misfit dislocations. In contrast, along MnAs[0001] a different strain relaxation mechanism is realized.[19] The $\sim 29\%$ misfit is released by a 4° tilt of the MnAs layer about the $[11\bar{2}0]$ axis.

Along MnAs$[11\bar{2}0]$ we again explore the interfacial configuration by depth-tunable GID. The GID profiles of the first-order and second-order reflections are shown in Fig. 7. The incidence angle is specified at the right of each curve. We observe satellites at both reflections. They appear when the incidence angle exceeds the critical angle, which confirms that they originate from the interface. A radial scan of the first-order reflection along the MnAs$[11\bar{2}0]$ direction does not show any satellites between the main peaks. However, a weak satellite peak, S_{-1}, is visible at an incidence angle of 0.6°, Fig. 7(a). The distance between the satellite and the substrate peaks is equal to the separation of the main peaks. In the second-order measurements [Fig. 7(b)], we see only one satellite between the main peaks. This is in contrast to the MnAs/GaAs(001) case where three satellites are present. The splitting of substrate, layer, and satellite peaks is again due to the coexistence of the α and β phases of MnAs as discussed in the preceding section.

The presence of the satellite reflections confirms that the misfit in the MnAs/GaAs(113)A interface is also released by a regular array of misfit dislocations. The period of the satellites, which is two times larger as compared to the MnAs/GaAs(001) case, gives half the spacing between the periodic misfit dislocations, $\Lambda = 2.45 \pm 0.05$ nm. The release of the same misfit by twice the number of the dislocations implies a Burger vector that is twice as small. This means that the in-plane component of the Burgers vector at the

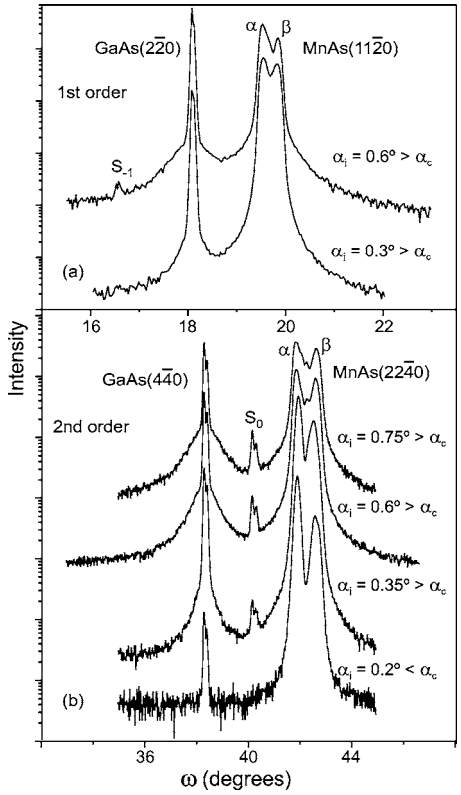

FIG. 7. Radial ($\omega/2\Theta$) scans recorded along the *a* axis of the MnAs/GaAs(113)A interface for different grazing incidence angles α_i. (a) First- and (b) Second-order reflection. The S_i indicate the satellites originating from the periodic array of misfit dislocations. The scans are recorded at room temperature. Peaks labelled α and β refer to the different phases of MnAs. The profiles are shifted vertically for clarity. X-ray energy, 10 keV.

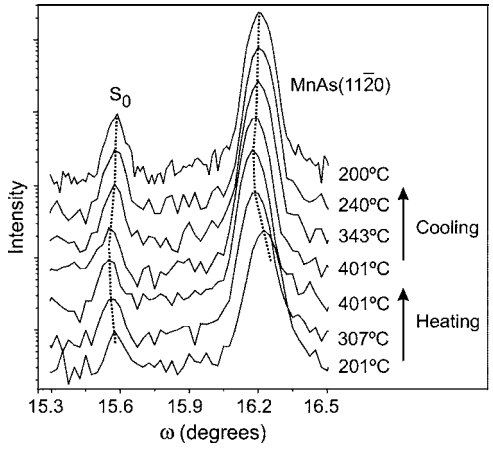

FIG. 8. Radial ($\omega-2\Theta$) scans along the MnAs[11$\bar{2}$0] direction measured in GID geometry during *in situ* post-growth annealing. The scans were recorded at a grazing incidence angle of 0.3°. The temperature is given to the right of each curve. For clarity, the curves are shifted in the vertical direction. The dotted lines on the curves are guides to the eye for the peak position at different temperatures. X-ray energy, 12 keV.

MnAs/GaAs(113)A interface is $\frac{1}{6}[11\bar{2}0]$, which is in agreement with Eq. (1). Referring to the GaAs lattice, the same Burgers vector is given by $\frac{1}{2}[1\bar{1}0]$, which is the smallest Burgers vector in the zinc-blende crystal structure.[39]

D. Effect of thermal annealing

We have investigated the effect of post-growth thermal annealing on the crystal quality of the MnAs layer as well as on the ordering of the dislocation array at the interface. The annealing was carried out *in situ* at 400 °C for 10 minutes with heating and cooling rates of 15 °C min^{-1}. The annealing was done without cooling the sample to room temperature after growth and in an arsenic-rich ambient to prevent As desorption from the MnAs surface. Growth and annealing are both carried out within the γ phase of MnAs. Radial scans along the MnAs[11$\bar{2}$0] direction were recorded during the annealing cycle (Fig. 8). The thermal expansion coefficient of γ-MnAs in the basal plane is $4.3\times10^{-5}\ \text{K}^{-1}$,[42] which is one order of magnitude larger than that of GaAs ($5.7\times10^{-6}\ \text{K}^{-1}$). Thus, upon heating, the MnAs(11$\bar{2}$0) peak shifts towards lower angles. The temperature dependence of the in-plane lattice parameter *a* during annealing is deduced from the MnAs peak position and shown in Fig. 9(a). A net increase of 0.43% for the in-plane lattice spacing is observed during heating to 400 °C, while the increase in lattice parameter due to thermal expansion is calculated to be 0.18%. The remaining 0.25% can be attributed to an annealing-induced relaxation of the layer. We cannot rule out the intermixing of Mn and Ga, which was found in an annealing study of MnAs film on GaAs(001) without As-rich environment.[43] However, we note that the lattice spacings in our experiment tend to the bulk MnAs values, which indicates a perfect crystal structure.

To investigate the effect of annealing on the in-plane order of the MnAs layer, we analyze the MnAs(11$\bar{2}$0) peak widths in the radial scans. The correlation length along MnAs[11$\bar{2}$0] as a function of annealing temperature is shown in Fig. 9(b). It is obtained from the FWHM of the peaks (corrected for the instrumental resolution) by using Scherrer's formula.[30] A net 20 % increase in the in-plane correlation length is observed, indicating a clear improvement in the crystal quality of the layer most probably by the removal of the defects at domain boundaries and the coalescence of smaller domains during annealing. Transverse scans of the MnAs peaks show a decrease in peak width from 0.43° before annealing to 0.24° after the thermal treatment. As discussed earlier, the width of the transverse scans is completely attributed to the in-plane mosaic spread. Therefore, the mosaic spread of the layer is reduced by almost 50%. The grains are less twisted around the surface normal, which also implies annihilation of defects at the grain boundaries. The integrated intensity of the MnAs peak, which should remain constant according to kinematical theory, increases at the same time by a factor of 1.8 [Fig. 9(c)]. This increase may be attributed to the enhancement of the crystal quality by increasing the order in the film, removal of lattice defects and distortions, which reduces the static Debye-Waller factor. Since the thermal expansion coefficient of

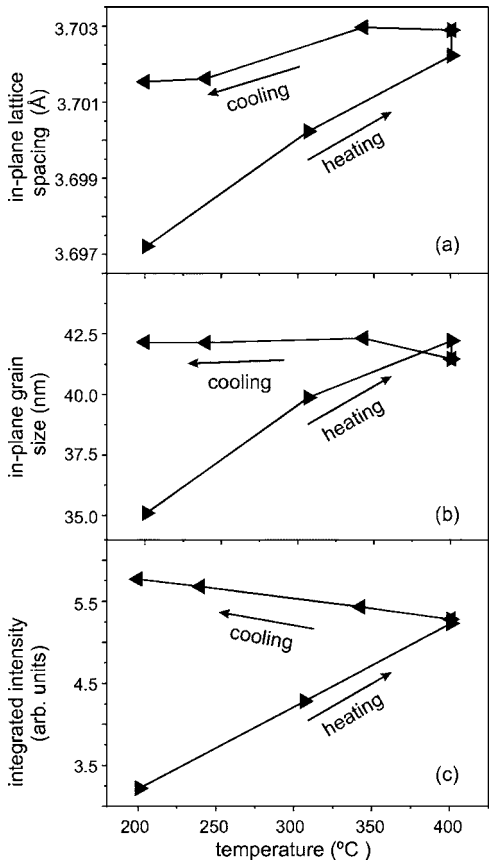

FIG. 9. The evolution of in-plane lattice spacing (a), in-plane grain size (b), and integrated intensity (c) along the *a* axis during *in situ* post-growth thermal annealing as a function of annealing temperature. The arrows indicate the direction of heating to 400 °C and subsequent cooling to 200 °C. The filled triangles pointing right represent the measurement during heating. The triangles pointing left represent the measurement during cooling.

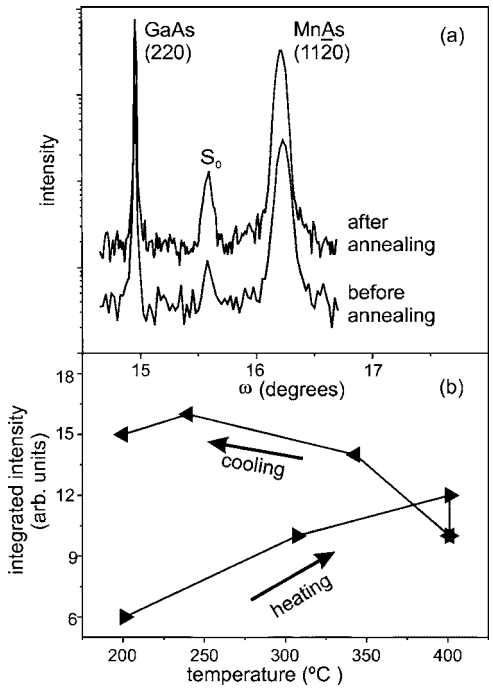

FIG. 10. (a) Radial ($\omega/2\Theta$) scans along the MnAs[11$\bar{2}$0] direction measured at 200 °C before and after annealing. (b) The evolution of integrated intensity of the S_0 satellite during annealing. The intensity increases 2.5 times during annealing. Arrows indicate the heating and cooling sequence. X-ray energy, 12 keV.

MnAs is notably larger than that of GaAs, the misfit decreases with rising temperature. The satellite peak, S_0, changes its position in the same way as the layer peak, as shown by the dotted lines in Fig. 8. The satellite peak always stays in the center between the layer and substrate peaks at all temperatures. Hence, the dislocation network changes its period to accommodate the lattice parameter misfit at a given temperature.

Figure 10(a) shows two diffraction curves, before and after annealing both at 200 °C. The integrated intensity of the satellite reflection S_0 is plotted as a function of annealing temperature in Fig. 10(b). The increase in integrated intensity by a factor 2.5 clearly indicates an improvement in the periodicity of the dislocation array.

IV. CONCLUSIONS

In conclusion, we find that the growth of MnAs on the GaAs(001) surface proceeds through the nucleation of almost relaxed MnAs islands starting from 4.2 ML, growth and coalescence of the islands. Misfit dislocations are introduced already at a nominal thickness of 6 ML directly at the interface before coalescence. The in-plane twist of the MnAs islands decreases continuously during growth.

Depth-resolved grazing incidence diffraction reveals an ordered array of misfit dislocations at the MnAs/GaAs(001) interface. These dislocations are interfacial edge dislocations with dislocation lines along the MnAs[0001] direction and the Burgers vector $\frac{1}{3}[11\bar{2}0]$. The separation between the dislocations is 4.95 ± 0.05 nm. The Burgers vector is equal to one lattice spacing along MnAs[11$\bar{2}$0] and represents the shortest possible perfect-dislocation Burgers vector in the hexagonal system. The Burgers vector lies in the plane of the interface and hence is very efficient in strain relaxation by allowing lateral gliding of the misfit dislocations. These results agree with TEM studies.[7]

At the MnAs/GaAs(113)A interface, the strain is also released by the formation of a regular dislocation array of the same orientation. The period of the dislocations is 2.45 ± 0.05 nm, which is exactly half of the period observed at the MnAs/GaAs(001) interface. The Burgers vector is $\frac{1}{6}[11\bar{2}0]$. The dislocation arrays change their periods according to the strain variation caused by the coexistence of the α and β phases of MnAs at room temperature. The intensity of the dislocation satellite along the CTR is measured and compared to model calculations. The inhomogeneous strain field of the misfit dislocation array is found to be confined at the interface within a thickness of 1.6 nm.

During annealing, the crystal quality of the MnAs layer improves drastically and a 0.25% relaxation of the in-plane lattice parameter *a* is observed. We find an increase in the

integrated intensity of the layer peak by a factor of 1.8, primarily due to the improved crystal quality due to the removal of defects during annealing. The mosaicity of the MnAs layer is reduced by almost 50%. The order of the dislocation array also improves due to annealing. The period of the dislocation network adjusts itself to the lattice parameter misfit at all temperatures investigated.

ACKNOWLEDGMENTS

The authors thank X. X. Guo, S. Behnke, C. Herrmann, and H-P. Schönherr for their valuable support in the experiments. The authors thank O. Brandt and B. P. Tinkham for critically reading the paper. This work is sponsored by the Bundesministerium für Bildung und Forschung of the Federal Republic of Germany.

*Electronic address: dillip@pdi-berlin.de

[1] S. Datta and B. Das, Appl. Phys. Lett. **56**, 665 (1990).
[2] G. A. Prinz, Science **282**, 1660 (1998).
[3] I. Žutić, J. Fabian, and S. D. Sarma, Rev. Mod. Phys. **76**, 323 (2004).
[4] E. Bauer, Z. Kristallogr. **110**, 372 (1958).
[5] John A. Venables, *Introduction to Surfaces and Thin Film Processes* (Cambridge University Press, Cambridge, UK, 2000).
[6] R. Hull and J. Bean, Crit. Rev. Solid State Mater. Sci. **17**, 507 (1994).
[7] A. Trampert, F. Schippan, L. Däweritz, and K. H. Ploog, Appl. Phys. Lett. **78**, 2461 (2001).
[8] D. K. Satapathy, B. Jenichen, V. M. Kaganer, W. Braun, L. Däweritz, and K. H. Ploog, J. Vac. Sci. Technol. B **24**, 2079 (2004).
[9] G. Springholz and K. Wiesauer, Phys. Rev. Lett. **88**, 015507 (2002).
[10] G. Renaud, P. Guénard, and A. Barbier, Phys. Rev. B **58**, 7310 (1998).
[11] R. Popescu, H. L. Meyerheim, D. Sander, J. Kirschner, P. Steadman, O. Robach, and S. Ferrer, Phys. Rev. B **68**, 155421 (2003).
[12] A. Bourret and P. Fuoss, Appl. Phys. Lett. **61**, 1034 (1992).
[13] A. Y. Babkevich, R. A. Cowley, N. J. Mason, S. Weller, and A. Stunault, J. Phys.: Condens. Matter **14**, 13505 (2002).
[14] R. Liu and F. A. Ponce, Appl. Phys. Lett. **83**, 860 (2003).
[15] M. Tanaka, J. P. Harbison, T. Sands, T. L. Cheeks, V. G. Keramidas, and G. M. Rothberg, J. Vac. Sci. Technol. B **12**, 1091 (1994).
[16] M. Tanaka, J. P. Harbison, M. C. Park, Y. S. Park, T. Shin, and G. M. Rothberg, J. Appl. Phys. **76**, 6278 (1994).
[17] F. Schippan, A. Trampert, L. Däweritz, and K. H. Ploog, J. Vac. Sci. Technol. B **17**, 1716 (1999).
[18] L. Däweritz, F. Schippan, A. Trampert, M. Kästner, G. Behme, Z. Wang, M. Moreno, P. Schützendübe, and K. H. Ploog, J. Cryst. Growth **227–228**, 834 (2001).
[19] L. Däweritz, L. Wan, B. Jenichen, C. Herman, J. Mohanty, A. Trampert, and K. H. Ploog, J. Appl. Phys. **96**, 5056 (2004).
[20] M. Kästner, L. Däweritz, and K. Ploog, Surf. Sci. **511**, 323 (2002).
[21] K. Akeura, M. Tanaka, M. Ueki, and T. Nishinaga, Appl. Phys. Lett. **67**, 3349 (1995).
[22] *Powder Diffraction File* (ICCD, Swarthsmoor, PA, 1977), No. PDF 280644.
[23] H. Okamoto, *Binary Alloy Phase Diagrams* (American Society of Metals, Metals Park, OH, 1990), Vol. 1, p. 293.
[24] I. K. Robinson and D. J. Tweet, Rep. Prog. Phys. **55**, 599 (1992).
[25] B. Jenichen, W. Braun, V. M. Kaganer, A. G. Shtukenberg, L. Däweritz, C.-G. Schulz, K. H. Ploog, and A. Erko, Rev. Sci. Instrum. **74**, 1267 (2003).
[26] I. K. Robinson, Phys. Rev. B **33**, 3830 (1986).
[27] M. Sauvage-Simkin, R. Pinchaux, J. Massies, P. Claverie, N. Jedrecy, J. Bonnet, , and I. K. Robinson, Phys. Rev. Lett. **62**, 563 (1989).
[28] M. Wassermeier, J. Sudijono, M. D. Johnson, K. T. Leung, B. G. Orr, L. Däweritz, and K. Ploog, Phys. Rev. B **51**, 14721 (1995).
[29] B. Jenichen, D. Satapathy, W. Braun, L. Däweritz, and K. H. Ploog, J. Appl. Phys. **96**, 6103 (2004).
[30] B. E. Warren, *X-Ray Diffraction* (Dover, New York, 1990).
[31] G. Renaud, A. Barbier, and O. Robach, Phys. Rev. B **60**, 5872 (1999).
[32] G. K. Williamson and W. H. Hall, Acta Metall. **1**, 22 (1953).
[33] W. C. Marra, P. Eisenberger, and A. Y. Cho, J. Appl. Phys. **50**, 6927 (1979).
[34] H. Dosch, B. W. Batterman, and D. C. Wack, Phys. Rev. Lett. **56**, 1144 (1986).
[35] V. M. Kaganer, B. Jenichen, F. Schippan, W. Braun, L. Däweritz, and K. H. Ploog, Phys. Rev. Lett. **85**, 341 (2000).
[36] V. M. Kaganer, B. Jenichen, F. Schippan, W. Braun, L. Däweritz, and K. H. Ploog, Phys. Rev. B **66**, 045305 (2002).
[37] M. Tanaka, Physica E (Amsterdam) **2**, 372 (1998).
[38] A. Trampert, Physica E (Amsterdam) **13**, 1119 (2002).
[39] J. P. Hirth and J. Lothe, *Theory of Dislocations* (Wiley, New York, 1982).
[40] T. Plake, M. Ramsteiner, V. M. Kaganer, B. Jenichen, M. Kästner, L. Däweritz, and K. H. Ploog, Appl. Phys. Lett. **80**, 2523 (2002).
[41] E. Vlieg, J. Appl. Crystallogr. **30**, 532 (1997).
[42] B. T. M. Willis and H. P. Rooksby, Proc. Phys. Soc. London, Sect. B **67**, 290 (1954).
[43] L. Däweritz, C. Herrmann, J. Mohanty, T. Hesjedal, K. H. Ploog, E. Bauer, A. Locatelli, S. Cherifi, R. Belkhou, A. Pavlovska, and S. Heun, J. Vac. Sci. Technol. B **23**, 1759 (2005).
[44] Such a curve is measured in GID geometry by keeping the angle between the source and the detector constant and equal to twice the Bragg angle of the diffracting plane while rotating the sample about the surface normal.